https://doi.org/10.31436/iiumej.v27i1.3970

Evaluating Mechanical and Conductivity of Graphene-Silver Hybrid Inks on Copper Substrate at Elevated Temperature

AHMAD ZAIFAZLIN ZAINORDIN[1,2], NOR AZMMI MASRIPAN[2], MUHD RIDZUAN MANSOR[2], CHONLATEE PHOTONG[3], ALAN WATSON[4], MOHD AZLI SALIM[2*]

[1]*Jabatan Kejuruteraan Mekanikal, Politeknik Sultan Haji Ahmad Shah, 25350 Kuantan, Pahang*
[2]*Fakulti Teknologi dan Kejuruteraan Mekanikal, Universiti Teknikal Malaysia Melaka, Malaysia*
[3]*Faculty of Engineering, Mahasarakham University, Thailand*
[4]*Power Electronics and Machines Centre, The University of Nottingham, UK Malaysia*

**Corresponding author: azli@utem.edu.my*

(Received: 3 October 2025; Accepted: 7 December 2025; Published online: 12 January 2026)

ABSTRACT: This study investigates the effect of temperature on the damping behaviour, stiffness, and natural frequency of hybrid conductive ink (HCI) printed on a copper (Cu) substrate. The HCI comprises graphene nanoplatelets (GNPs), silver flakes (SF), and silver acetate (SA). The objective is to evaluate the HCI's electrical conductivity and mechanical properties under varying thermal conditions. The HCI paste was formulated with a specified ratio of organic solvents, terpineol, and 1-butanol and cured in an oven at 260°C for 3 hours. The baseline droplet ratio was set at 1:1, and three Cu samples with varied HCl compositions were printed using a 60 µm mesh stencil process. The terpineol concentrations were changed while the 1-butanol droplet remained constant. The samples were then tested for electrical conductivity at room temperature using a two-point probe, in accordance with IEEE Std 118-1978, followed by mechanical behaviour testing using an ASTM E756-05 impact test. Furthermore, the samples were exposed to a range of temperature tests to evaluate mechanical and electrical conductivity under thermal stress. The results showed that the baseline composition exhibited minimal resistance and resistivity across the temperature range, with an average resistance of ≤ 0.2 Ω and a resistivity of ≤ 0.8 Ω · mm, respectively. The baseline composition also exhibited reduced stiffness and damping, with natural frequencies of 10.90, 1.40 kN/m, and 37.51 Hz across the samples. Therefore, the baseline composition exhibits relatively good electrical and mechanical properties for applications in flexible electronics.

ABSTRAK: Kajian ini meneliti kesan suhu terhadap sifat redaman, kekakuan, dan frekuensi semula jadi bagi dakwat konduktif hibrid (HCI) yang dicetak pada substrat kuprum (Cu). HCI ini terdiri daripada graphene platelet nano (GNP), serpihan perak (SF), dan perak asetat (SA). Objektif kajian ini adalah bagi menilai kekonduksian elektrik dan sifat mekanikal HCI di bawah keadaan haba berbeza. Pes HCI dibangunkan dengan nisbah tertentu pelarut organik, terpineol dan 1-butanol, dan dikeringkan dalam ketuhar pada suhu 260ºC selama tiga jam. Nisbah titisan asas ditetapkan pada 1:1, dan tiga sampel Cu dengan komposisi HCI berbeza telah dicetak menggunakan proses stensil jaring 60 µm. Kepekatan terpinol diubah manakala titisan 1-butanol dikekalkan pada kadar yang sama. Sampel-sampel tersebut kemudiannya diuji bagi kekonduksian elektrik pada suhu bilik menggunakan probe Dua-Titik mengikut kod ujian piawaian IEEE Std 118-1978 dan diteruskan dengan ujian sifat mekanikal menggunakan ujian impak ASTM E756-05. Tambahan, sampel telah terdedah kepada pelbagai ujian suhu bagi menilai kekonduksian mekanikal dan elektrik di bawah tekanan haba. Dapatan kajian menunjukkan bahawa komposisi asas menunjukkan rintangan dan kerintangan minimum sepanjang julat suhu, dengan purata rintangan ≤ 0.2 Ω dan kerintangan ≤ 0.8 Ω/mm.

Komposisi asas juga menunjukkan sifat mekanikal dengan kekakuan berkurangan, tingkah laku redaman, dan frekuensi semula jadi masing-masing sebanyak 10.90, 1.40 kN/m, dan 37.51 Hz merentasi sampel. Oleh itu, komposisi asas menunjukkan sifat elektrik dan mekanikal yang agak baik bagi aplikasi elektronik fleksibel.

KEYWORDS: *Hybrid conductive ink, graphene, resistivity, damping, stiffness, frequency*

1. INTRODUCTION

Conductive ink is an advanced material used in various electronic applications, characterized by its ability to conduct electricity while being printable on flexible substrates [1]. It typically consists of conductive particles, such as silver (Ag), copper (Cu), or carbon, and solvents, which enhance electrical conductivity and stability [2]. Its versatility and ease of application make it suitable for the increasing demand for advanced technology in the Internet of Things era [3]. Furthermore, conductive ink is widely used in applications such as electronic components, flexible displays, wearable electronics, and smart packaging [4]. Recent research has demonstrated the potential of HCI, which integrates different conductive materials to achieve higher performance [4]. For example, Ag-Cu hybrid inks have demonstrated improved conductivity and cost-effectiveness compared to pure Ag inks [5]. In addition, the inks have been developed for optimal efficiency in circuit printing, with formulations that facilitate easy batch manufacturing and adaptability with various printing methods.

The impact of temperature on conductive ink is significant, affecting its electrical characteristics and stability. Previous studies demonstrate that different temperatures can affect the resistivity and performance of conductive inks, especially inks formulated with GNP and Ag nanoparticles [6]. Furthermore, the curing technique for GNP/Ag inks at low temperatures enhances conductivity and adhesion, minimising thermal damage to sensitive surfaces [7]. The graphene modified with oleic acid exhibits excellent electrical conductivity, with the optimised ink formulation achieving low resistance at room temperature [8]. Moreover, increased temperatures can lead to thermal degradation of temperature-sensitive substrates, limiting the applicability of conventional metallic inks that require high sintering temperatures, especially for biomaterials [9]. The balance between achieving conductivity while preventing damage is important, as high temperatures may damage the substrate's integrity [10]. This requires innovative ink formulations that allow for lower curing temperatures.

Conductive ink has demonstrated significant advances in conductivity and flexibility; however, there remains a research gap regarding its mechanical properties that influence electrical conductivity, particularly damping behaviour, stiffness, and natural frequency. Numerous studies have concentrated on electrical performance, examining the mechanical behaviour of conductive ink under dynamic conditions [11-14]. Besides, the importance of this gap arises from the fact that electronic devices frequently encounter mechanical stresses, including bending, stretching, and impact, which can influence their electrical conductivity [11]. Conductive inks have exhibited resilience through extensive bending cycles, indicating their suitability for dynamic applications such as human motion detection [15]. Besides, an inconsistency impacts the advancement of flexible electronics, where accurate mechanical properties are required for performance and durability [16].

Excessive vibration can affect the performance, reliability, and lifespan of electronic devices. The effects of vibration arise from various sources, including mechanical motion, environmental conditions, and operational components. The relationship between damping and stiffness significantly influences their natural frequency, as evidenced by various studies [17,18]. The natural frequency is influenced by material properties and structural

configurations, which can be quantified using experimental and numerical methods. Next, mechanical operations, such as torsion and bending, and environmental factors, such as temperature and humidity, can degrade electronic device performance. The researcher investigates the effects of GNP/Ag resistivity under torsional loading. After 5000 cycles, an increase in resistance is observed, attributable to material degradation [19]. Furthermore, cyclic torsion can lead to microcracks and defects in the ink layer, which correlates with increased resistivity [20]. Compared with torsion tests, bending tests show that resistivity increases after repeated motion, indicating degradation of electrical properties [21]. Given the highlighted limitations, it is vital to study the mechanical characteristics of conductive ink, including damping and stiffness, as well as natural frequencies, to optimise the mixture formulation.

Despite the increasing utilisation of GNP and Ag in HCI inks in emerging flexible electronics, existing studies have not sufficiently demonstrated how formulation-dependent thermal-mechanical and electrical properties translate into performance requirements at the device level [22,23]. The current literature primarily focuses on isolated material characterisation, with limited correlation with real operational demands, such as vibration tolerance, stiffness stability, and electrical continuity under dynamic loading. Consequently, a knowledge gap persists in establishing a direct linkage between material microstructure, processing conditions, and their functional implications in flexible electronic applications. This work aims to examine the effect of temperature on the electrical conductivity and mechanical properties, including damping, stiffness, and natural frequency, of HCI composed of GNP, Ag, and SA printed on Cu substrates. The study begins with an assessment of the impact of different terpineol-to-butanol droplet ratios on electrical conductivity at varied temperatures, followed by an investigation of mechanical properties to determine damping behaviour, stiffness, and natural frequency. The test is conducted to establish correlations between electrical and mechanical properties and to determine the optimal mixture composition for improved conductivity and stability under temperature and vibration conditions.

2. MATERIALS AND METHODS

2.1. Raw Material of Hybrid Conductive Ink

The primary conductive materials used in the formulation of HCI are GNP, SF, and SA, all sourced from Sigma-Aldrich. Ethanol, 1-butanol, and terpineol serve as solvents to ensure the ink is printable, adheres well to substrates, and meets performance standards under varying conditions. The HCI powder and paste are prepared following the methods described in previous studies [24]. Next, the material specifications for the HCI development process are stated in Table 1.

Table 1. The raw material in HCI development

Materials	Details
GNP	Average particle size of 25 µm with a molar mass of 12.01 g/mol
SF	Average particle size of ≤10 µm with a molar mass of 107.87 g/mol
SA	99% of purity with a molar mass of 166.91 g/mol
Ethanol	Denatured 99.99% with a molar mass of 46.07 g/mol
1-butanol	99.9% butyl alcohol with a molar mass of 74.12 g/mol
Terpinol	Monoterpene alcohol with a molar mass of 154.25 g/mol

This study used 25 µm particle-size GNP fillers, whose small particle size and powdered morphology facilitate integration into formulations, offering advantages across numerous applications [25]. Similarly, Sigma-Aldrich SF with 99.99% trace-metal purity was utilized to

https://doi.org/10.31436/iiumej.v27i1.3970

improve conductivity when combined with carbon-based materials. The SA serves as a filler material to enhance the conductivity and adhesion of GNP and Ag dispersion through synthesis methods [26,27]. In addition, the HCI formulation contains organic solvents, including ethanol, terpineol, and 1-butanol. Ethanol is used to disperse GNPs and SF in the ink uniformly and to prevent clumping. Terpineol and 1-butanol enhance drying control and adhesion, thereby providing uniform printed ink layers. Their controlled evaporation improves viscosity control, thereby establishing smooth conductive pathways and minimizing defects, thereby improving ink performance.

2.2. Preparation of Hybrid Powder

Figure 1 illustrates a comprehensive methodology for preparing fine HCl powder via a combination of chemicals and processing techniques. The procedure begins with the formulation of a mixture containing 0.005 g of GNP and 5 ml of ethanol, which is sonicated for 10 minutes. The sonication process employs ultrasonic waves to achieve complete dispersion of the GNP in the ethanol solvent, resulting in a uniform suspension and preventing agglomeration [28].

Next, 0.4292 g of SF is added to the mixture, followed by 1 h of sonication to promote uniform dispersion and interfacial interaction between SF and GNP. Subsequently, 0.042 g of SA is added to the mixture, which is sonicated for an additional hour to ensure uniform dispersion of SA. The mixture is subsequently heated to 70 ºC on a hot plate while being stirred at 200 rpm until the ethanol has evaporated. After stirring, the fine HCl powder was transferred to a small container and cured at 250 °C for 1 hour to remove residual ethanol and solidify the powder. After curing for 1 hour, the HCl powder was manually ground in a mortar and pestle until a fine powder formed. The fine HCl powder will be placed in a container for preparing the HCl paste.

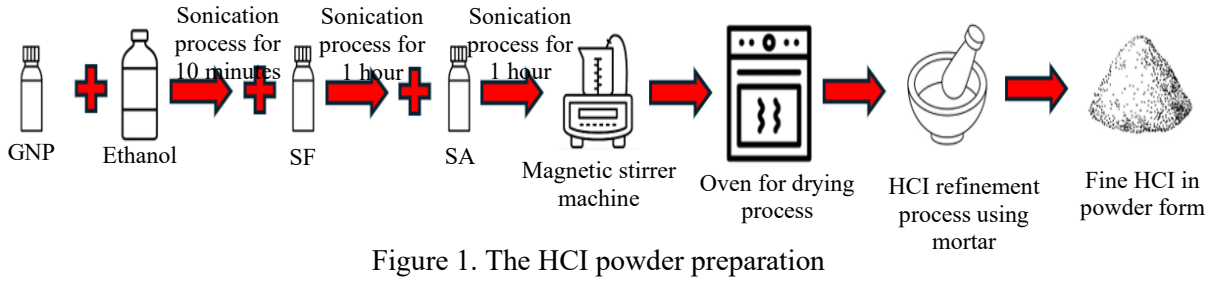

Figure 1. The HCI powder preparation

2.3. Preparation of HCI Paste and Sample

The process starts with the mixture of fine HCl powder and two solvents, terpineol and 1-butanol, as depicted in Figure 2. The mixture is subsequently thoroughly mixed with a Thinky Mixer to ensure uniform dispersion, prevent agglomeration, and eliminate air bubbles. The solvents facilitate proper paste formation, while the Thinky Mixer ensures uniformity and accuracy in substrate printing. Next, a mesh stencil is used to apply the HCI paste to the substrate. A squeegee is used to apply ink to the substrate surfaces, producing five-point ink samples.

Table 2 outlines the formulation for HCI as printed on the substrate surface. The droplet ratios of the three HCI samples differ, with the baseline ratio for terpineol and butanol set at 1:1. In this study, the number of terpineol droplets varies, whereas the quantity of 1-butanol remains constant. Three samples, labeled S1, S2, and S3, each represent a different quantity of

https://doi.org/10.31436/iiumej.v27i1.3970

droplets. Sample S1 is associated with 5T10B, S2 with 10T10B, and S3 with 15T10B as stated in Table 2.

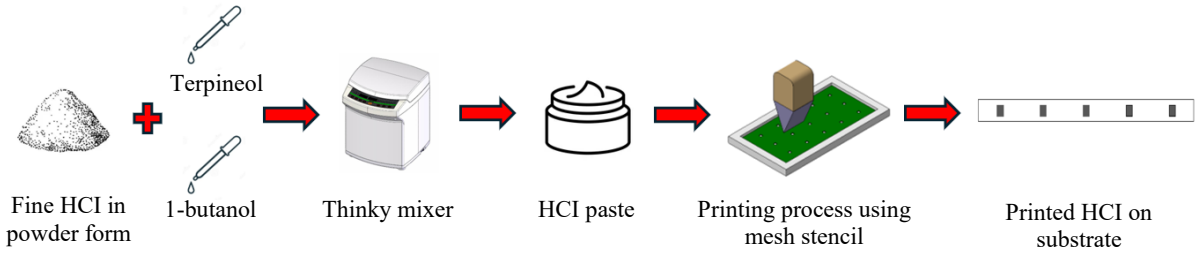

Figure 2. The HCI Paste and Sample Fabrication

Table 2. The HCI Powder and Paste Formulations

Sample	GNP (g)	Ethanol (ml)	SF (g)	SA (g)	Baseline ratio between terpineol and 1-butanol (1 droplet = 0.325 ml)
5T10B	0.005	5	0.4292	0.042	0.5:1
10T10B	0.005	5	0.4292	0.042	1:1
15T10B	0.005	5	0.4292	0.042	1.5:1

The HCI configuration was printed onto a Cu substrate during preparation, prior to electrical and mechanical testing, as illustrated in Figure 3. The Cu substrate measures 120 mm in length and 10 mm in width. A mesh stencil is used as a guide to print ink with a grid dimension of 3.5 mm by 3.5 mm and a thickness of 60 µm ± 2 µm. The printed sample had a 20 mm gap between all of them. A printed section is highlighted with an expanded view, illustrating details of its dimensions and sample placement.

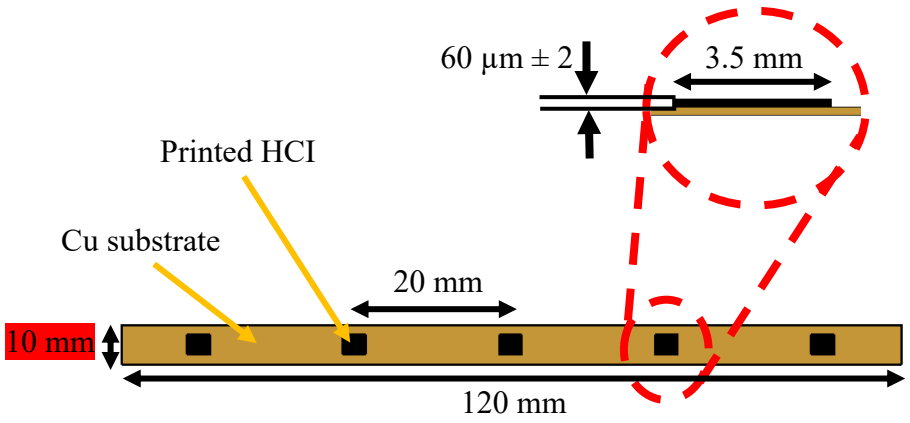

Figure 3. Printed HCI Sample Specification

2.4. Curing Process for HCI Samples

The curing process of printed HCI is depicted in Figure 4, which can influence its electrical conductivity. Three HCI samples with different mixture compositions undergo curing in a UF55 Universal oven chamber at 260 °C for three hours. The oven is utilised owing to its efficient heat distribution and consistency throughout the heating process. Additionally, this curing procedure is designed to ensure adequate adhesion and stabilisation of the printed HCI paste on the substrate.

https://doi.org/10.31436/iiumej.v27i1.3970

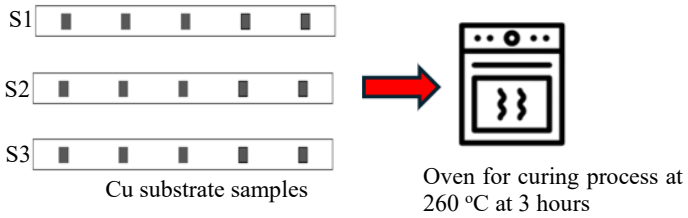

Figure 4. Substrate sample curing process

2.5. The HCI Sample under Various Temperature Effects

After curing, the samples are placed in a heating chamber to measure their electrical conductivity at controlled temperatures, as illustrated in Figure 5. The samples are positioned on the non-conductive glass surface within a heating chamber maintained at approximately 25 ºC. The temperature and humidity sensors are located within the heating chamber to precisely monitor temperature and humidity. Subsequently, a heating tube is positioned at the top of the heating chamber to promote uniform heat distribution, and the temperature control module regulates the temperature. The temperature was set for each test, starting at 30 °C and increasing in 10 °C increments to 60 °C. Subsequently, electrical conductivity measurements were obtained using the Two-Point probe method at each assigned temperature interval, and this procedure was repeated for all samples.

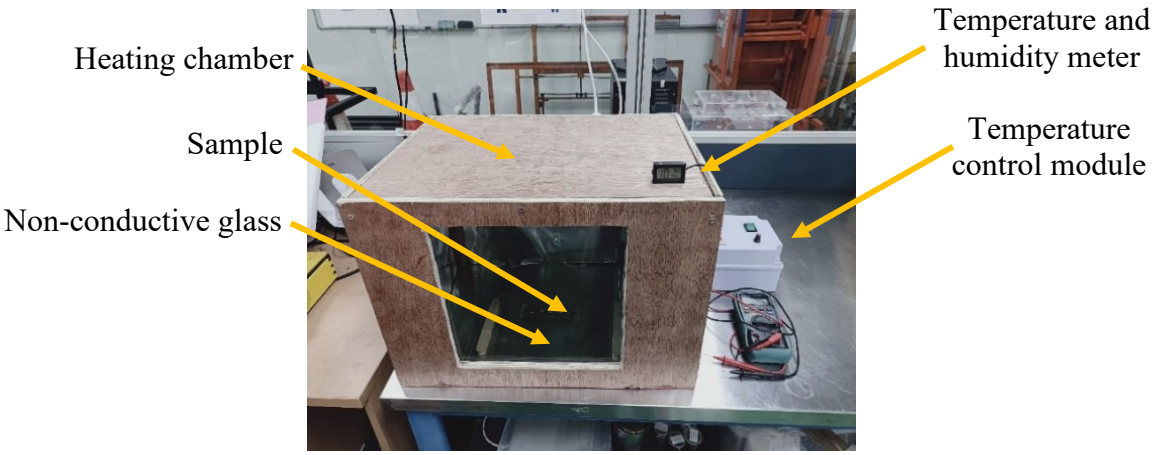

Figure 5. Sample characteristics using a heating chamber with temperature control

2.6 Resistance Measurement using Two-Point Probe

The Two-Point probe method is a simple technique for determining electrical conductivity in terms of resistance, as illustrated in Figure 6. This approach implements the standard test code of IEEE Std 118-1978, using two metallic probes that make direct contact with the printed ink surface to measure resistance.

https://doi.org/10.31436/iiumej.v27i1.3970

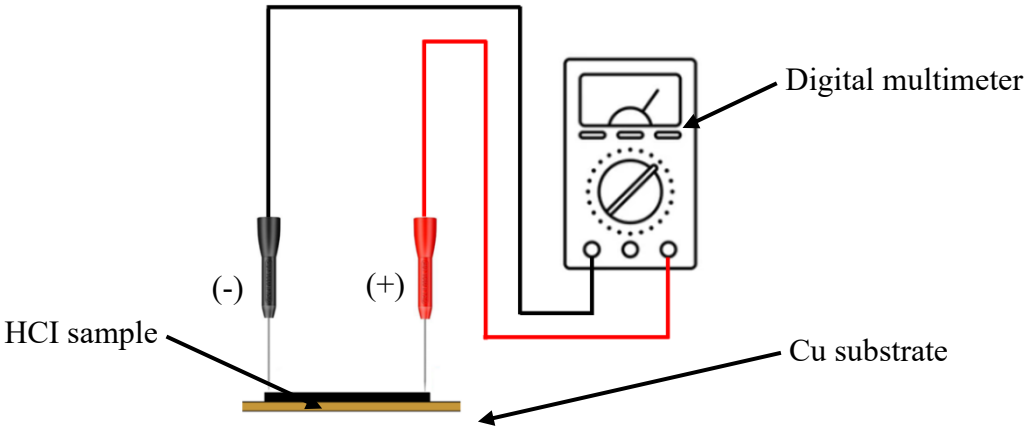

Figure 6. Two-Point probe measurement procedure

Through the resistance data collected, the resistivity was derived through theoretical calculations as outlined below:

$$\rho = \frac{RA}{L} \tag{1}$$

where, R is a resistance measurement, A is the HCI sample area, and L is the length of GNP. In this study, the HCI sample has dimensions of 3.5 mm in length and width. Next, the area (A) is calculated using the equation:

$$A = wL \tag{2}$$

where w is the width and L is the length of the sample. Next, the measurements are conducted at multiple points on the sample to ensure precision in the conductive layer. The probe-specified measurement locations are (1.1, 1.2), (2.1, 2.2), and (3.1, 3.2), as illustrated in Figure 7.

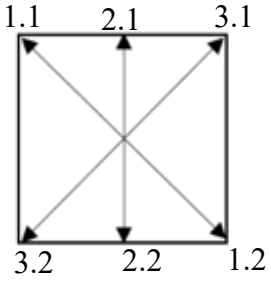

Figure 7. Testing Points for Printed HCI Samples

2.7. Damping, Stiffness, and Natural Frequency Measurements

The impulse hammer test is a fundamental method for exciting mechanisms during mobility measurements. This is a straightforward method to address the challenges of achieving consistent outcomes. The experiment aims to determine the mechanical characteristics of the printed HCI layer on the Cu substrate surfaces bonded to the aluminum beam (Al beam) after thermal exposure and to establish the correlation between temperature and the sample's mechanical properties.

https://doi.org/10.31436/iiumej.v27i1.3970

The experimental procedure begins with sample preparation, in which the Cu substrate is securely attached to the Al beam. The Al beam is fixed at one end, while the other end is allowed to vibrate freely, as seen in Figure 8. An accelerometer is attached to the free end to gather vibration data. At the same time, the impulse hammer is connected to the Data Acquisition System (DAQ) model QUADRO to record the applied force, ensuring synchronization with the accelerometer's measurements. Furthermore, the sample is assessed in accordance with ASTM E756-05 to determine the mechanical properties of HCI, including its damping behaviour, stiffness, and natural frequencies under specified impact loads.

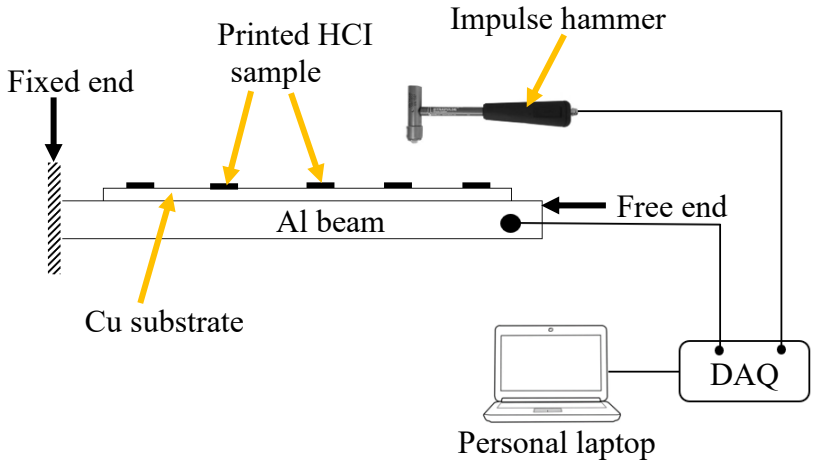

Figure 8. Schematic diagram for vibrational testing

During the experiment, the impulse hammer and accelerometer are calibrated to ensure precise force application and response measurement. Next, the DYTRAN impulse hammer, with a reference sensitivity of 5.21 mV/lb · F, generates an impulse force determined by its mass and velocity. The DYTRAN accelerometer, with a reference sensitivity of 10.12 mV/g, measures the resultant vibrations. Both sensors require calibration before testing to ensure accurate measurements.

The Al beam used in this work has a density of 2.7 g/cm³, a Young's modulus of 69 GPa, and a Poisson's ratio of 0.33, and its mechanical behaviour under axial stress is examined. The material shows a yield strength of 275 MPa and an ultimate tensile strength of 310 MPa, indicating the highest stress it can sustain before failure. Furthermore, the material demonstrates a thermal conductivity of 167 W/m·K, rendering it efficient in heat dissipation. The coefficient of thermal expansion is 23.6×10^{-6}/K, indicating a modest thermal expansion. A Brinell hardness of 95 signifies moderate resistance to indentation and abrasion. The measurements of the Al beam are 240 mm in length, 3 mm in width, and 19 mm in height. The equations for these characteristics, obtained from impact load responses, are shown below.

$$F = kx \tag{3}$$

In this equation, F denotes the impact force (N), k signifies the stiffness (N/m), and x indicates the displacement (m) resulting from the applied force. The stiffness (k) is determined by dividing the applied force by the corresponding displacement, representing the material's resistance to deformation under impact load. The Natural frequency (f_n) can be determined using the equation shown below:

$$f_n = \frac{1}{2\pi}\sqrt{\frac{k}{m}} \tag{4}$$

https://doi.org/10.31436/iiumej.v27i1.3970

where m is the mass of the beam in kg. The damping ratio (ζ) may be computed using the formula shown below:

$$\zeta = c/2f_n \quad (5)$$

3. RESULTS AND DISCUSSION

The experiment was conducted by varying the samples' temperature in a heat chamber, and the data were recorded using the two-point probe method. The averages and error bars for resistance and resistivity of HCI GNP/Ag are shown in Table 3, considering temperature effects and humidity. The sample's mechanical properties are subsequently examined to determine its damping behaviour, stiffness, and natural frequency following temperature variations.

Table 3. Averages and Error Bar for Resistance and Resistivity of the HCI GNP/Ag

Temperature (ºC)/ Humidity (%)	**Average resistance (Ω)**			**Average resistivity (Ω.mm)**			**Error bar**					
							5% of Average Resistance (Ω)			**5% of Average Resistivity (Ω.mm)**		
Mixture	5T 10B	10T1 0B	15T1 0B	5T 10B	10T1 0B	15T1 0B	5T 10B	10T1 0B	15T1 0B	5T 10B	10T1 0B	15T1 0B
25/ (71)	0.55	0.45	0.40	1.91	1.59	1.40	0.03	0.02	0.02	0.10	0.08	0.07
30/ (66)	1.04	0.17	0.12	3.38	0.61	0.42	0.06	0.01	0.01	0.17	0.03	0.02
40/ (64)	0.31	0.17	0.15	1.07	0.61	0.54	0.02	0.01	0.01	0.05	0.03	0.03
50/ (63)	0.19	0.17	0.22	0.68	0.42	0.40	0.01	0.01	0.01	0.03	0.02	0.02
60/ (59)	0.23	0.19	0.56	0.79	0.68	1.96	0.01	0.01	0.03	0.04	0.03	0.10

Figure 9 depicts the average resistance and resistivity of GNP/Ag HCl as functions of temperature for three formulation combinations: 5T10B, 10T10B, and 15T10B. The increased effectiveness of the 10T10B formulation can be attributed to its stability across a range of temperature conditions. The results indicate that the electrical resistance and resistivity of all formulations varied minimally over the temperature range of 30-60 °C, indicating a high degree of thermal stability. Nevertheless, 10T10B consistently exhibited the lowest resistance and resistivity across the samples within this temperature range. This suggests that the material's composition facilitates efficient electron transport, even at elevated temperatures. The carefully calibrated amounts of conductive fillers (GNP and Ag) and the terpineol-to-1-butanol droplet ratio are likely instrumental in establishing a robust conductive network that maintains its integrity under thermal stress. Consequently, 10T10B exhibits not only elevated electrical conductivity but also consistent performance, making it particularly suitable for applications characterized by frequent temperature fluctuations.

Conversely, 5T10B first exhibits an increase in resistance and resistivity at 30 °C, followed by a decrease as the temperature rises to 60 °C, resulting in a resistivity difference of 23%. In HCI, materials containing nanoparticles, such as GNP and Ag, must form continuous networks to enable efficient electron transport [6]. Higher temperatures promote particle dispersion and connectivity, thereby reducing resistance [29]. In addition, resistivity can increase due to the formation of isolated particles caused by insufficient heat.

Compared to the lowest temperature, 15T10B shows a small increase in resistance of around 40% as the temperature rises. This is because substrate temperature affects electrical properties, thereby altering ion distribution and crystal orientation [30]. The temperature of the Cu substrate significantly influences electrical properties; as the deposition temperature

https://doi.org/10.31436/iiumej.v27i1.3970

increases, sheet resistance decreases, thereby enhancing conductivity. The conductivity of films deposited at 200 ºC is low, according to a previous HCI study. However, conductivity improves owing to larger grain sizes at 250 °C and 300 °C, which are higher temperatures [31]. According to this study, the number of droplets can influence particle dispersion. As shown in Figure 9, when the droplet ratio of terpineol is reduced, the mixture of 5T10B exhibits high resistivity at 30 ºC, whereas 15T10B exhibits high resistivity at 60 ºC. This demonstrates the importance of terpineol in enhancing drying control and adhesion, thereby producing smooth, conductive pathways and minimizing defects, thus improving ink performance.

Table 4. Average and Percentage Difference in Conductivity of the HCI GNP/Ag

Temperature (ºC)/ Humidity (%)	**Average conductivity (S/mm)**			**Percentage Difference in Conductivity (%)**		
Mixture	5T 10B	10T 10B	15T 10B	5T 10B	10T 10B	15T 10B
25/ (71)	0.52	0.63	0.71			
30/ (66)	0.30	1.65	2.38	2.38	1.62	2.35
40/ (64)	0.93	1.65	1.86	1.86	1.62	1.62
50/ (63)	1.48	2.38	2.52	2.52	2.78	2.55
60/ (59)	1.26	1.48	0.51	0.51	1.35	-0.28

Table 4 demonstrates that the temperature and humidity influence the electrical conductivity of the HCI GNP/Ag formulations across all sample mixtures. At 25ºC, all samples exhibit moderate conductivity, with 15T10B showing the highest value owing to its greater proportion of conductive fillers, which enhances the formation of interconnected pathways between GNP and Ag particles. As the temperature increases to 30°C and 40°C, the 10T10B and 15T10B formulations exhibit a sharp increase in conductivity. This improvement occurs because heat softens the polymer binder and reduces ink viscosity, enabling better packing, enhanced particle contact, and lower interfacial energy barriers [6]. Humidity within this range may promote slight matrix softening, enabling greater compression without affecting structural integrity. The highest conductivity for all formulations occurs at 50°C, indicating an optimal thermal window in which the microstructure achieves maximum particle alignment and strong percolation networks while maintaining mechanical stability. Beyond this point, performance declines. At 60°C, resistivity increases and conductivity decreases, particularly in 15T10B, indicating structural deterioration due to excessive heat, such as microcracking, thermal expansion mismatch, or over-softening of the binder, which disrupts established conductive pathways.

The characteristics of the solvent mixtures primarily govern differences among the formulations. Terpineol is more effective than 1-butanol because its higher boiling point and slower evaporation rate keep the ink in a wet state for longer, allowing GNP and Ag particles to reorganize into a denser, more continuous conductive network [24]. Its better dispersing ability also helps achieve a more uniform particle distribution during drying. In contrast, 1-butanol evaporates quickly, reducing the time available for particle rearrangement and resulting in a less compact structure. Therefore, formulations with higher terpineol content, particularly 15T10B, exhibit higher conductivity at moderate temperatures and more stable thermally driven network formation.

https://doi.org/10.31436/iiumej.v27i1.3970

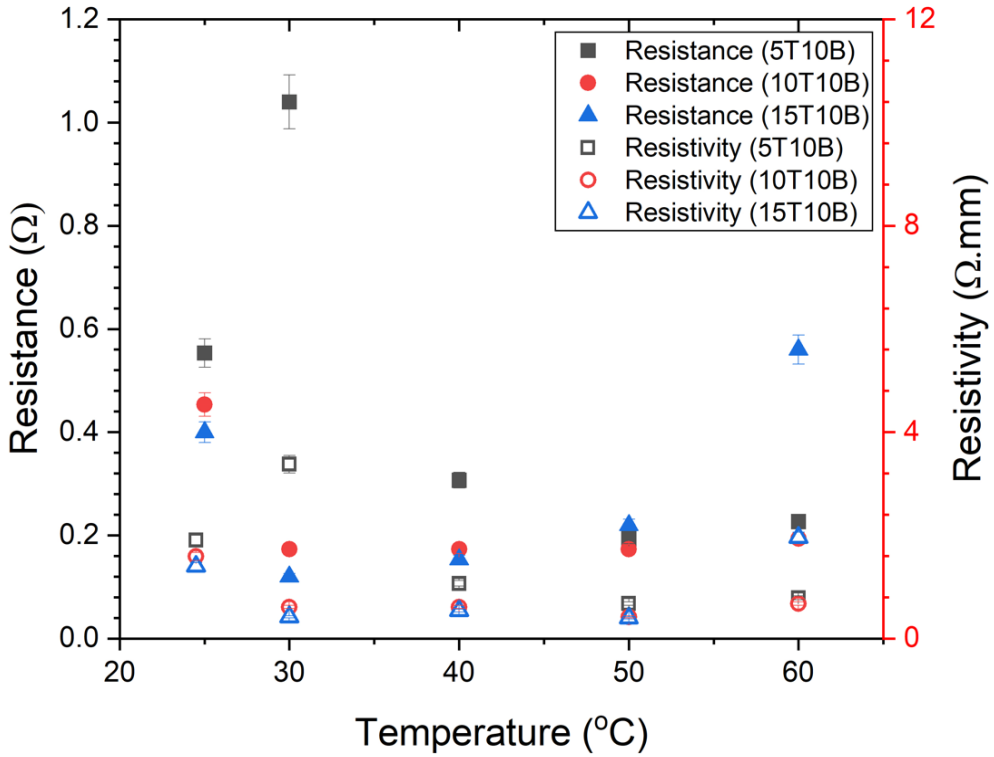

Figure 9. Average Resistance and Resistivity of HCI GNP/Ag

Next, the error bars for the average resistance and resistivity of HCI composed of GNPs and Ag under varying temperature and humidity conditions are presented in Table 3. The results show that measurement error decreases as temperature rises from 25°C to 60°C, indicating improved stability and uniformity of the conductive film at elevated temperatures. Among the tested mixtures, 10T10B consistently exhibits the smallest error bars for both resistance and resistivity, indicating a more stable and homogeneous conductive network than 5T10B and 15T10B. The higher variability observed at lower temperatures, particularly in the 5T10B sample, may be attributed to incomplete curing and weaker interconnections between conductive particles, which lead to fluctuations in electrical pathways [32]. Conversely, increasing temperature enhances the adhesion and interfacial bonding between GNP and Ag flakes, thereby improving electron mobility and reducing measurement uncertainty. The slight decrease in humidity with increasing temperature also contributes to reduced moisture interference, further stabilizing electrical performance [6].

Based on the results, the HCI GNP/Ag combination is a promising formulation because it exhibits excellent electrical conductivity while minimizing substrate heat damage, making it suitable for various applications. Among the studied formulations, 10T10B appears to be the most successful, owing to its well-balanced composition of GNP, SF, SA, and solvents. This composition not only performs well electrically but is also highly stable, retaining consistent conductivity even under varying temperatures. The overall component balance in 10T10B appears to maximise both efficiency and durability, which is essential for utilisation in flexible and wearable electronics.

The sample is then examined for mechanical properties, focusing on damping behaviour, stiffness, and natural frequency, using an impact-testing method. The data obtained during testing includes impulse hammer response, and displacement is derived by integrating the acceleration data. Furthermore, the damping, stiffness, and natural frequency parameters are obtained from theoretical calculations, as specified in Equations (3) to (5). Table 5 presents the

https://doi.org/10.31436/iiumej.v27i1.3970

mechanical parameters of the samples, including an Al beam and HCI-mixture samples 5T10B, 10T10B, and 15T10B, subjected to impact loads. Five impact points have been identified in the sample, which closely resemble those in the printed sample. The data were obtained from the experimental results and processed using MATLAB.

Table 5. Measurement results for damping, stiffness, and natural frequency

Sample	Impact load (N)	Displacement (m)	Stiffness (kN/m)	Natural frequency (Hz)	Velocity (m/s)	Damping ratio (ζ)
Al beam	27.38	0.240	0.05	10.04	0.17	2.84
5T10B	28.25	0.013	2.17	43.13	0.003	37.91
10T10B	24.13	0.017	1.40	37.51	0.012	10.9
15T10B	27.60	0.010	3.45	55.01	0.01	8.92

In flexible and wearable electronic systems, damping, stiffness, and natural frequency are essential mechanical properties that directly influence device reliability and performance. Damping characterizes a material's ability to dissipate mechanical energy, which is crucial for minimizing vibrations and mechanical shocks. High damping capacity helps protect sensitive electronic components from fatigue or failure under repeated mechanical stress, particularly in motion-intensive applications such as healthcare wearables and soft robotics. For stiffness, or the resistance to deformation under applied force, it must be carefully tuned. Excessive stiffness may hinder flexibility, making the device uncomfortable or impractical for wearable use, while insufficient stiffness can compromise structural stability and the protection of embedded circuitry. Optimizing stiffness ensures mechanical durability while maintaining sufficient compliance for stretchability and conformability. The natural frequency is the rate at which a system vibrates in response to an external disturbance. If this frequency aligns with external vibration sources, resonance can occur, drastically increasing stress and potentially leading to structural failure or erratic performance. Hence, controlling the natural frequency through careful design of material geometry, mass, and stiffness is essential to avoid resonance. Together, these mechanical parameters underpin the design of robust, high-performance flexible electronics capable of withstanding real-world mechanical challenges.

Table 6. Measurement results for damping, stiffness, and natural frequency

Sample	Stiffness (kN/m)	Natural frequency (Hz)	Damping ratio (ζ)	Error bar (5%)		
				Stiffness (kN/m)	Natural frequency (Hz)	Damping ratio (ζ)
5T10B	2.17	43.13	37.91	0.11	2.16	0.14
10T10B	1.40	37.51	10.9	0.07	1.88	1.90
15T10B	3.45	55.01	8.92	0.17	2.75	0.55

Table 6 summarises the measured stiffness, natural frequency, and damping ratio for the three HCI formulations, together with their respective ±5% error bars. These parameters are crucial because they reflect the coated Cu substrate's ability to resist vibrational excitation, dissipate mechanical energy, and maintain structural–electrical stability under dynamic operating conditions. The 15T10B formulation recorded the highest stiffness value of 3.45 kN/m and the highest natural frequency of 55.01 Hz, indicating that the higher GNP and Ag filler loading produced a mechanically stiffer coating and consequently a higher resonant response; however, this sample also showed the lowest damping ratio of 8.92, which reflects a reduced capability to dissipate vibrational energy. In contrast, the 5T10B sample showed a moderate stiffness value of 2.17 kN/m and a natural frequency of 43.13 Hz, yet achieved the

https://doi.org/10.31436/iiumej.v27i1.3970

highest damping ratio of 37.91, suggesting that lower filler concentration permitted greater viscoelastic mobility and improved energy absorption. The 10T10B formulation recorded the lowest stiffness (1.40 kN/m) and a natural frequency of 37.51 Hz, while exhibiting a moderately low damping ratio of 10.9. Overall, the trend indicates that each formulation produces a different balance between structural rigidity and energy dissipation, confirming that formulation composition strongly governs the thermal-mechanical performance of the HCI.

Figure 10 illustrates the effects of stiffness and average resistivity across various mixture samples, emphasising the disparities in mechanical and electrical properties. The 5T10B formulation demonstrates the highest stiffness, surpassing 3.45 kN/m, while its resistivity remains moderate. By contrast, the 10T10B sample exhibits the lowest stiffness (approximately 1.40 kN/m) and resistivity, indicating excellent electrical conductivity. The 15T10B mixture exhibits a stiffness of roughly 2.17 kN/m, with a resistivity that exceeds that of 10T10B but is lower than that of 5T10B. The results indicate that the formulation's composition significantly influences both mechanical and electrical performance. Similarly, as reported in previous studies, the incorporation of GNP into epoxy/glass fiber composites enhances the overall stiffness, resulting in an increase in natural frequencies by up to 8.05%, while the damping ratio decreases by more than 35% [33]. Although increased stiffness, as demonstrated by 5T10B, provides improved resistance to deformation, it may restrict flexibility and key characteristics of wearable and flexible electronics.

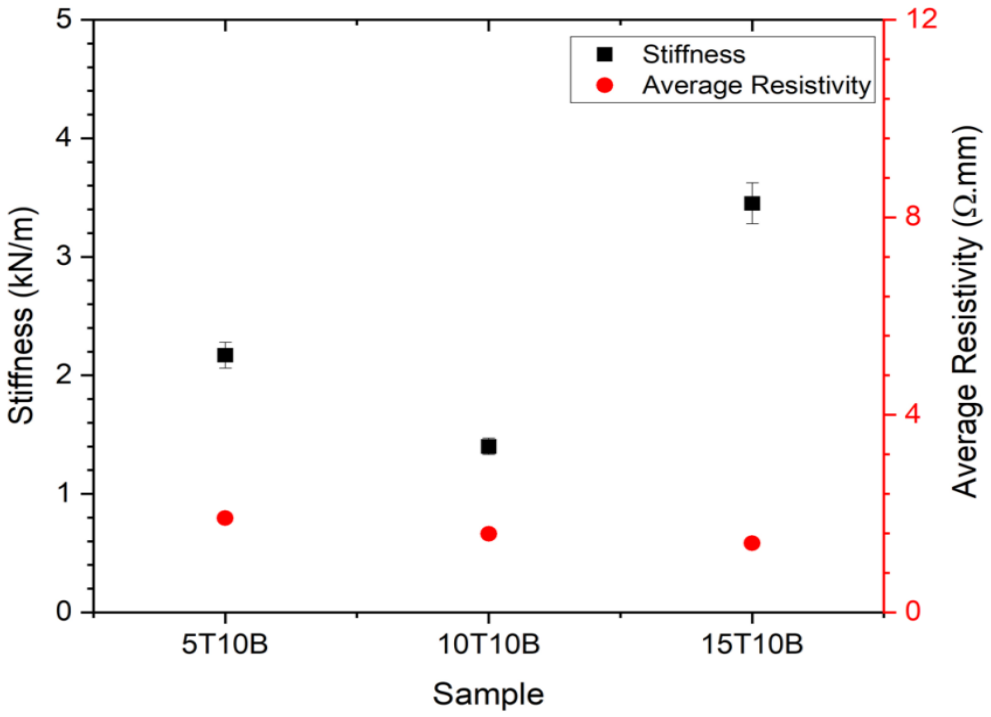

Figure 10. Comparison between stiffness and average resistivity at various mixture samples

Moreover, excessive rigidity can adversely impact damping performance, diminishing materials' ability to absorb mechanical shocks or vibrations [34]. The reduced rigidity of 10T10B facilitates enhanced damping, making it more appropriate for dynamic applications characterised by movement and vibration. Furthermore, natural frequency is intrinsically linked to stiffness; increased stiffness elevates the natural frequency, which may result in resonance under specific conditions. The 10T10B formulation, characterised by reduced stiffness and possibly diminished natural frequency, may mitigate such problems, hence improving device dependability. Moreover, the 10T10B formulation provides the optimal

https://doi.org/10.31436/iiumej.v27i1.3970

combination of mechanical compliance, damping capacity, and electrical conductivity among the evaluated samples. This is because the 10T10B formulation has a balanced filler concentration and film thickness, which enables the formation of an optimal percolation network for stable and efficient charge transport [24,35]. It provides an ideal combination of mechanical flexibility and electrical conductivity, ensuring consistent electrical performance and enhanced damping capacity [36].

Figure 11 depicts the correlation between natural frequency and average resistivity across various mixture samples. The results indicate significant differences in both characteristics across the multiple formulations. The 5T10B sample exhibits the highest average resistivity, exceeding 3.38 Ω·mm, despite a relatively low natural frequency of approximately 43 Hz. The 10T10B sample has the lowest resistivity, approximately 0.42 Ω·mm, and the lowest natural frequency, approximately 40 Hz. Meanwhile, the 15T10B sample exhibits an increase in natural frequency to approximately 55 Hz, along with an average resistivity. Based on the results, it is essential to recognise that the natural frequency depends on both the material's stiffness and mass. An elevated natural frequency typically indicates a more rigid structure, which may enhance resistance to deformation but could also reduce the flexibility and damping required for specific electronic applications. In contrast, reduced natural frequencies, as shown in 10T10B, may arise from elastic structures that are better suited to dynamic and flexible applications.

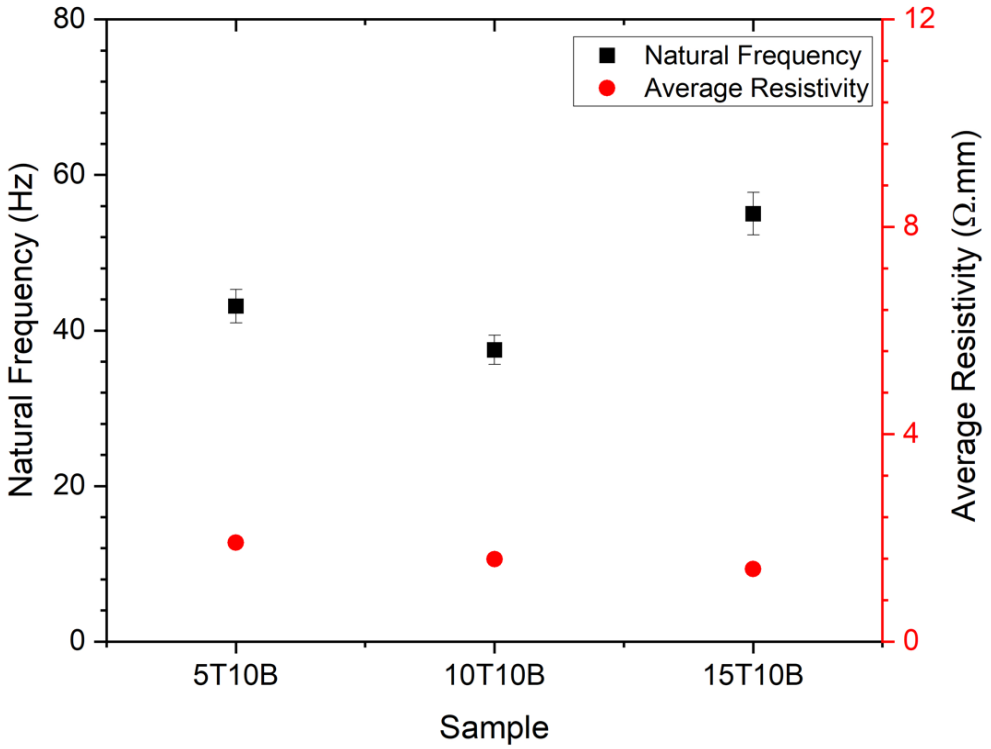

Figure 11. Comparison between natural frequency and average resistivity at various mixture samples

The conductive network inside the formulation determines the impact on resistivity. A lower natural frequency may indicate a more flexible, continuous conductive path that enhances electron transport, thereby reducing resistance. Consequently, the 10T10B sample's combination of low natural frequency and low resistivity indicates ideal structural and electrical stability. The findings suggest that modifying mixture composition can effectively optimise both mechanical and electrical properties, essential for developing high-performance HCI formulations for flexible and wearable electronics.

https://doi.org/10.31436/iiumej.v27i1.3970

Through applying an impact force of 27.38 N, the Al beam demonstrates a maximum displacement of 0.240 m, a minimum stiffness of 0.0452 kN/m, and a minimum natural frequency of 10.04 Hz, as illustrated in Figure 12. Conversely, the HCI samples exhibit significantly higher stiffness and natural frequency, and lower displacement under comparable impact loads. When applying an impact load of 28.25 N, the 5T10B sample exhibits a minimum displacement of 0.013 m, yielding a stiffness of 2.17 kN/m and a natural frequency of 43.13 Hz. The 10T10B sample exhibits a marginally reduced impact load of 24.13 N and a displacement of 0.0172 m, yielding a stiffness of 1.40 kN/m and a natural frequency of 37.51 Hz. At the 27.6 N impact load, the 15T10B sample exhibits the minimal displacement of 0.008 m, the maximum stiffness of 3.45 kN/m, and the highest natural frequency of approximately 55.01 Hz relative to all other samples.

The results reveal that the HCI samples outperform the Al beam in stiffness and natural frequency, primarily due to variations in material composition and thermal treatment. These mechanical enhancements are attributed to the improved structural framework and interfacial bonding within the hybrid composite. Notably, an inverse relationship between stiffness and displacement is observed: higher stiffness results in reduced deformation under identical stress conditions. This aligns with fundamental mechanical principles: a stiffer material resists shape changes more effectively, enhancing structural stability but often at the cost of reduced damping capacity. The data further indicate that as stiffness increases, the natural frequency also rises. This correlation suggests that stiffer materials are more resistant to oscillatory disturbances, thereby offering greater mechanical stability. However, this comes with a trade-off, where increased stiffness generally corresponds to a lower damping ratio, meaning the material is less effective at dissipating energy under dynamic loads. These characteristics have critical implications for applications involving vibration or cyclic mechanical stress. Figure 12 illustrates this dynamic by showing the inverse correlation between stiffness and both displacement and the damping ratio, demonstrating that deformation decreases as stiffness increases.

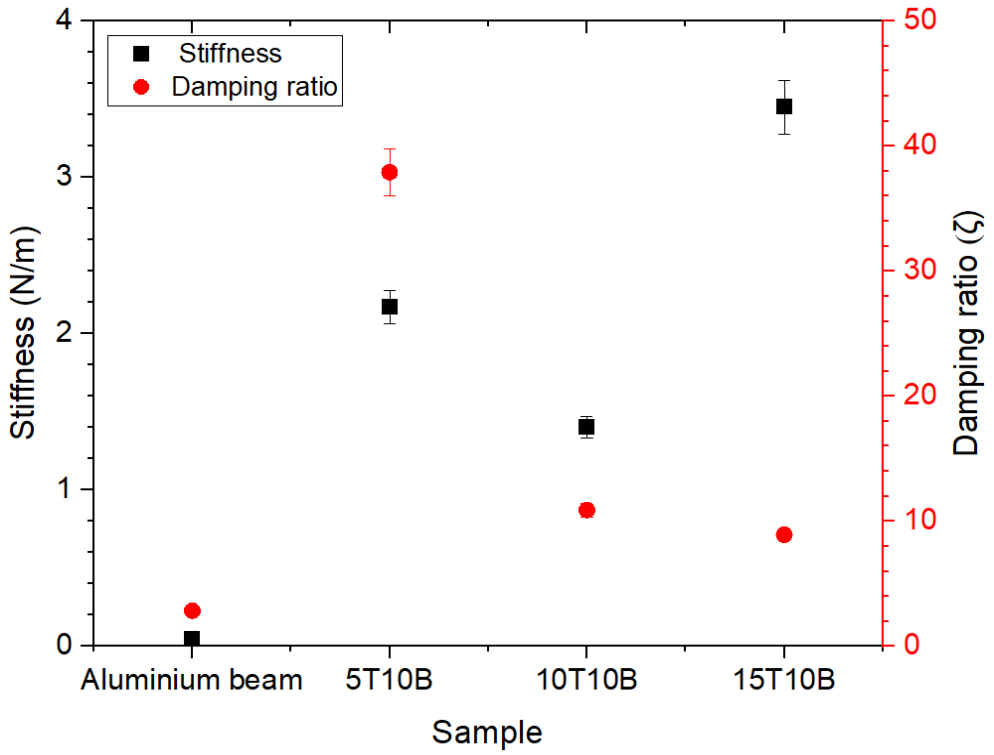

Figure 12. Comparison between stiffness and damping ratio at various mixture samples

https://doi.org/10.31436/iiumej.v27i1.3970

Figure 13 presents SEM micrographs of the HCI samples after vibration exposure. Before morphological examination, the HCI specimens were thermally cured at 260 ºC for 3 hours and subsequently subjected to impact testing using an Al beam. The microstructure was observed at ×2000 magnification. During testing, the vibration impact acted five times simultaneously on the printed film, which is known to induce particle rearrangement and affect interfacial stability along the conductive pathways. Figure 13(a) depicts the 5T10B formulation, exhibiting noticeable pore formation. This phenomenon is attributed to the solvent ratio, which reduces packing density and promotes void formation, thereby weakening the conductive network. In contrast, Figure 13(b) depicts the 10T10B formulation, displaying well-coated metallic particles with strong interparticle bonding and the absence of discernible particle boundaries, attributes that indicate an efficient and flexible conductive network. Figure 13(c) shows the 15T10B sample, in which the SEM image reveals a well-dispersed HCI structure that forms a continuous and stable conductive network even after combined impact–vibration exposure. Despite the presence of small voids, these discontinuities may disrupt some conductive pathways, explaining the relatively higher susceptibility to conductivity degradation under vibration-assisted mechanical deformation. The microstructural stability under combined impact-vibration conditions indicates that the 10T10B composition maintains an ideal balance between mechanical integrity and electrical conductivity, making it more adaptable than the other formulations.

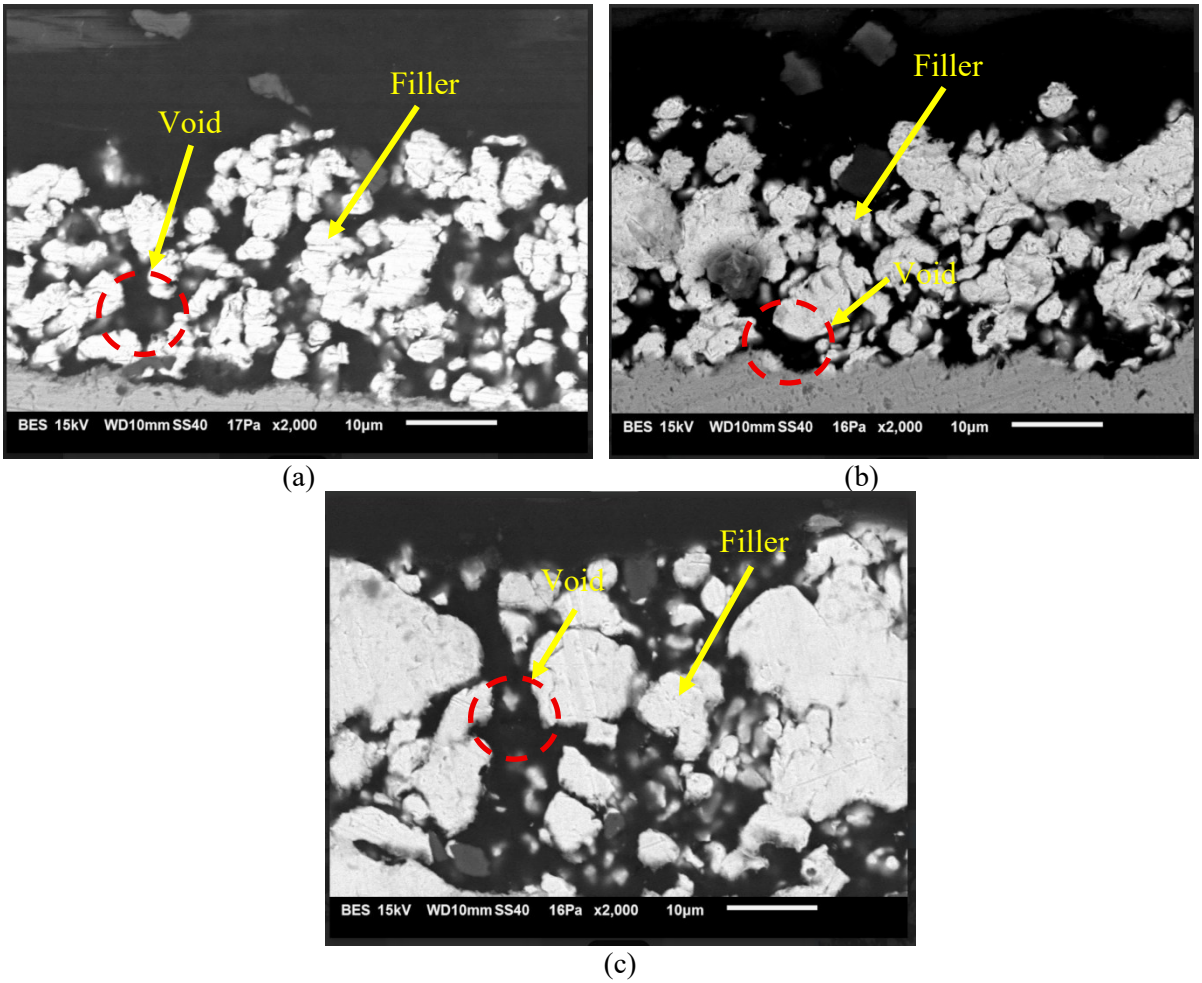

Figure 13. SEM images of each sample after impact testing.

Moreover, the study highlights how the mechanical and electrical properties of GNP/Ag HCI formulations are strongly influenced by material composition and thermal behavior. As temperature increases, the polymer binder softens, allowing GNP and Ag fillers to come into closer contact, thereby improving particle dispersion and strengthening both conductive networks. This effect is most evident in the 10T10B formulation, which achieves an effective balance of stiffness, damping, and conductivity. Its moderate stiffness and lower natural frequency enhance damping capacity and flexibility, making it suitable for wearable or flexible electronic applications. The 15T10B formulation exhibits more stiffness and a higher natural frequency, resulting in less damping and reduced mechanical flexibility. The improved stiffness observed at moderate temperatures arises from thermally induced matrix reduction, which enables more uniform stress redistribution and better particle interlocking. The solvent effects further reinforce these outcomes: formulations with higher terpineol content, such as 15T10B, develop denser and more uniform particle networks during curing owing to terpineol's slower evaporation and better dispersive capability [37]. These consolidated microstructures provide greater thermal stability but also increase rigidity. Conversely, the rapid evaporation of 1-butanol yields less compact networks, making mechanical properties more sensitive to thermal softening [38]. The results show that optimal mechanical performance is achieved when thermal activation enhances network formation without inducing excessive stiffness, a balance most effectively demonstrated by the 10T10B formulation.

4. CONCLUSIONS

This study demonstrates that the initial composition of HCI printed on the Cu substrate displays excellent electrical conductivity with low resistance and resistivity across the investigated temperature range. Furthermore, the mechanical properties, such as stiffness, natural frequency, and damping behaviour, are comparatively lower, suggesting an agreement between electrical and mechanical performance. The results indicate that preserving the baseline composition enhances electrical conductivity while providing acceptable mechanical properties. Nevertheless, modifications to the HCI composition, particularly changes in terpineol content, adversely affect both electrical and mechanical stability. This highlights the importance of precise formulation modifications to maintain conductivity and structural integrity for reliable applications. Overall, the findings indicate that HCI on Cu substrates can achieve a good balance of damping performance, structural stiffness, and electrical conductivity. These characteristics demonstrate their suitability for use in flexible electronic interfaces that require suppression of mechanical vibration and reliable signal transmission. In addition, the property stability demonstrated in this study indicates strong potential for scalable formulation refinement and integration into industrial-scale printed electronic manufacturing processes, particularly for lightweight sensor assemblies, smart structural components, and next-generation vibration-responsive circuitry. Thus, the baseline composition exhibits relatively good electrical and mechanical properties for applications in flexible electronics.

ACKNOWLEDGMENTS

The authors would like to express their sincere gratitude to the Advanced Academia Industry Collaboration Laboratory (AiCL), Fakulti Teknologi dan Kejuruteraan Mekanikal, Universiti Teknikal Malaysia Melaka, and the Department of Mechanical Engineering, Politeknik Sultan Haji Ahmad Shah, Kuantan, Pahang.

REFERENCES

[1] Yanan W (2019). Flexible substrate, manufacturing method of flexible substrate and flexible display device, (2019).

[2] Haixin C, Ganghui L, Hui G, (2020). Graphene composite conductive ink and preparation method thereof.

[3] Romero EC, Sanchez Hernandez S, Acosta AM, (2023). Development of Carbon-Based Conductive Inks with Resistant Response for Potential Use in Flexible Sensors with IoT Technology. 2023 IEEE Colombian Caribbean Conference (C3), IEEE p. 1–5.

[4] Osváth Z, Pálinkás A, Piszter G, Molnár G, (2020). Synthesis and Characterization of Graphene–Silver Nanoparticle Hybrid Materials. Materials, 13(20):4660. Doi: 10.3390/MA13204660.

[5] Bobsin A, Rodrigues TC, Fernandes IJ, Ferreira SB, Peter CR, Hasenkamp W, et al., (2024). Copper and silver microparticles for high-performance conductive inks in electronic chip shielding. Materials Chemistry and Physics, 315:129007. Doi: 10.1016/j.matchemphys.2024.129007.

[6] Noor NM, Salim MA, Masipan NA, Md. Saad A, Photong C, Akop MZ, (2024). Correlation Effect on Different Temperature-Humidity Range of Highly Thermal GNP/AG/ SA Conductive Ink. International Journal of Integrated Engineering, 16(6).

[7] Muhammad Hisyamuddin Hussin, Nor Azmmi Masripan, Mohd Azli Salim, Adzni Md. Saad, Chonlatee Photong, (2024). Electric Symphony: Unveiling the Potential of Reduced-Temperature Cured Conductive Ink. Journal of Advanced Research in Applied Mechanics, 120(1):72–84. Doi: 10.37934/aram.120.1.7284.

[8] Le TT, Bui HHT, Dinh AKP, Van DV, Ho QD, Thi HAN, et al., (2022). Room Temperature-Sintering Conductive Ink Fabricated from Oleic-Modified Graphene for the Flexible Electronic Devices. ChemistrySelect, 7(4). Doi: 10.1002/slct.202104249.

[9] Zhou Y, Xu Z, Bai H, Knapp CE, (2023). Room Temperature Electronic Functionalization of Thermally Sensitive Substrates by Inkjet Printing of a Reactive Silver-Based MOD Ink. Advanced Materials Technologies, 8(8). Doi: 10.1002/admt.202201557.

[10] Liu T, Guo R, Fu Y, Zhao J, Ning H, Fang Z, et al., (2022). Morphological Regulation of Printed Low-Temperature Conductive Ink. Langmuir, 38(32):9955–66. Doi: 10.1021/acs.langmuir.2c01249.

[11] Zulfiqar S, Saad AA, Ahmad Z, Yusof F, Bachok Z, (2023). Structural Analysis of Silver-Based Conductive Ink Under Cyclic Loading. In: Mohd Salleh, M.A.A., Che Halin, D.S., Abdul Razak, K., Ramli, M.I.I., editors. Proceedings of the Green Materials and Electronic Packaging Interconnect Technology Symposium, Singapore: Springer Nature Singapore p. 211–9.

[12] Walsh P, (2023). Structural Analysis of Silver-Based Conductive Ink Under Cyclic Loading:211–9. Doi: 10.1007/978-981-19-9267-4_25.

[13] Koshi T, Nomura K, Yoshida M, (2019). Requirements for Durability Improvement of Conductive Patterns Permeated in Textiles under Cyclic Tensile Deformation. Micromachines, 10(11):721. Doi: 10.3390/MI10110721.

[14] Du H, Xue T, Xu C, Kang Y, Dou W, (2018). Improvement of mechanical properties of graphene/substrate interface via regulation of initial strain through cyclic loading. Optics and Lasers in Engineering, 110:356–63. Doi: https://doi.org/10.1016/j.optlaseng.2018.04.026.

[15] Wu P, He H, (2024). Integrating High-Performance Flexible Wires with Strain Sensors for Wearable Human Motion Detection. Sensors, 24(15):4795. Doi: 10.3390/s24154795.

[16] Cordill MJ, Glushko O, Putz B, (2016). Electro-Mechanical Testing of Conductive Materials Used in Flexible Electronics. Frontiers in Materials, 3. Doi: 10.3389/fmats.2016.00011.

[17] Azam SA, Fragoso A, (2020). Experimental and Numerical Simulation Study of the Vibration Properties of Thin Copper Films Bonded to FR4 Composite. Applied Sciences, 10(15):5197. Doi: 10.3390/app10155197.

[18] OLINGHERU R-G, OLARIU A-B, PRAISACH Z-I, (2024). The influence of stiffness on the dynamic behavior of a PCB enclosure. Studia Universitatis Babeș-Bolyai Engineering,:130–6. Doi: 10.24193/subbeng.2024.1.13.

[19] Ismaniza Ismail, Mohd Azli Salim, Nor Azmmi Masripan, Adzni Md. Saad, Mohd Zaid Akop, Chew Kit Wayne, et al., (2024). Effect of Torsional Load on Electrical and Mechanical Properties/Behaviour of Stretchable GNP-Ag Conductive Ink. Journal of Advanced Research in Applied Mechanics, 117(1):22–34. Doi: 10.37934/aram.117.1.2234.

[20] Hussain MA, Salim MA, Masripan NA, Md. Saad A, Akop MZ, Photong C, (2024). Investigation of Functional Ageing of GNP/Ag Conductive Ink under Torsional Conditions. International Journal of Integrated Engineering, 16(2). Doi: 10.30880/ijie.2024.16.02.034.

[21] Ismaniza Ismail, Mohd Azli Salim, Nor Azmmi Masripan, Adzni Md. Saad, Mohd Zaid Akop, Chew Kit Wayne, et al., (2024). Resistivity of Graphene/Silver Hybridization Conductive Ink on Bending Test. Journal of Advanced Research in Applied Mechanics, 120(1):27–39. Doi: 10.37934/aram.120.1.2739.

[22] Zhang Y, Wu H, Liu L, Yang Y, Zhang C, Duan J, (2024). Crack-Based Composite Flexible Sensor with Superhydrophobicity to Detect Strain and Vibration. Polymers, 16(17):2535. Doi: 10.3390/polym16172535.

[23] Lu A, Zhao L, Liu Y, Li Z, Xiong D-B, Zou J, et al., (2020). Enhanced Damping Capacity in Graphene-Al Nanolaminated Composite Pillars Under Compression Cyclic Loading. Metallurgical and Materials Transactions A, 51(4):1463–8. Doi: 10.1007/s11661-020-05632-4.

[24] Jori SH, Salim MA, Masripan NA, Md. Saad A, Chonlatee P, (2024). Effect of Butanol and Terpinol as a Solvents in GNP/SA Conductive Ink. Journal of Advanced Research in Applied Mechanics, 120(1):62–71.

[25] Li W, Yan J, Wang C, Zhang N, Choy TH, Liu S, et al., (2022). Molecule bridged graphene/Ag for highly conductive ink. Science China. Materials, 65(10):2771–8. Doi: 10.1007/s40843-022-2064-8.

[26] Dubey RK, Shukla S, Hussain Z, (2023). Green Synthesis of Silver Nanoparticles; A Sustainable Approach with Diverse Applications. Chinese Journal of Applied Physiology,:e20230007. Doi: 10.62958/j.cjap.2023.007.

[27] Rafique M, Sadaf I, Rafique MS, Tahir MB, (2017). A review on green synthesis of silver nanoparticles and their applications. Artificial Cells, Nanomedicine, and Biotechnology, 45(7):1272–91. Doi: 10.1080/21691401.2016.1241792.

[28] Kasim NFA, Idris WFW, Abdullah AH, Yusoh K, Ismail Z, (2019). The preparation of graphene ink from the exfoliation of graphite in pullulan, chitosan and alginate for strain-sensitive paper. International Journal of Biological Macromolecules,. Doi: 10.1016/j.ijbiomac.2019.10.251.

[29] Rezaga BFY, Balela MDL, (2024). Conductive Inks with Chemically Sintered Silver Nanoparticles at Room Temperature for Printable, Flexible Electronic Applications. Key Engineering Materials, 983:9–16. Doi: 10.4028/p-DAaz5z.

[30] Zhang K, Kong W, Wang Q, Xuan T, Cheng F, Chang A, (2019). Effect of substrate temperature on structure, cationic distribution and electrical properties of MnCo0.2Ni0.1Mg0.6Al1.1O4 thin films. Journal of Materials Science: Materials in Electronics, 30(15):14200–6. Doi: 10.1007/s10854-019-01787-y.

[31] Koshy AM, Sudha A, Yadav SK, Swaminathan P, (2023). Effect of substrate temperature on the optical properties of DC magnetron sputtered copper oxide thin films. Physica B: Condensed Matter, 650:414452. Doi: 10.1016/j.physb.2022.414452.

[32] Inoue M, Suganuma K, (2005). Effect of curing conditions on the interconnect properties of isotropic conductive adhesives composed of an epoxy-based binder. 2005 Conference on High Density Microsystem Design and Packaging and Component Failure Analysis, IEEE p. 1–6.

[33] Veenapani R, Ananda Kumar KV, Pavana B S, (2024). Impact of Graphene Reinforcement Upon Damping Properties of Epoxy/Glass Hybrid Composites. Journal of Scientific Research and Technology,:12–9. Doi: 10.61808/jsrt136.

[34] Geethamma VG, Asaletha R, Kalarikkal N, Thomas S, (2014). Vibration and sound damping in polymers. Resonance, 19(9):821–33. Doi: 10.1007/s12045-014-0091-1.

[35] Mohd Azli Salim, Norida Mohammad Noor, Nor Azmmi Masripan, Adzni Md. Saad, Mohd Zaid Akop, Chew Kit Wayne, et al., (2024). Effect of GNP/Ag Stretchable Conductive Ink on Electrical Conductivity. Journal of Advanced Research in Applied Mechanics, 119(1):1–12. Doi: 10.37934/aram.119.1.112.

[36] Sato R, Kawakita J, Chikyow T, Sakamoto Y, (2017). Mechanical-Electrical Behaviour of Conductive Polymer / Metal Composite for Flexible Interconnect. ECS Meeting Abstracts, MA2017-02(52):2205–2205. Doi: 10.1149/MA2017-02/52/2205.

[37] Ahmed MR, Mirihanage W, Potluri P, Fernando A, (2023). Highly Stable Graphene Inks Based on Organic Binary Solvents. Particle & Particle Systems Characterization, 40(2). Doi: 10.1002/ppsc.202200153.

[38] Kosasih EA, Hakim AAR, Hussein M, (2018). Analysis of butanol droplet evaporation using modified stagnant film model. p. 020009.